NISTIR 5873

# INTRACYCLE EVAPORATIVE COOLING IN A VAPOR COMPRESSION CYCLE

**Byung Soon Kim**
**Piotr A. Domanski**

**September 1996**

**U.S. Department of Commerce**
Michael Kantor, *Secretary*
Technology Administration
Mary L. Good, *Under Secretary for Technology*
National Institute of Standards and Technology
Arati Prabhakar, *Director*

***Prepared for:***
U.S. Department of Energy
William Noel, *Project Manager*
Office of Building Technology
Building Equipment Division Laboratory
Energy Efficiency and Renewable Energy
1000 Independence Ave., SW
Washington, DC 20585

**Abstract**

The temperature glide of zeotropic mixtures during phase change provides the opportunity to limit throttling losses of the refrigeration cycle by intracycle evaporative cooling of the refrigerant leaving the condenser. Intracycle evaporative cooling is similar to the use of a liquid-line/suction-line heat exchanger with the difference that a two-phase low-pressure refrigerant, instead of superheated vapor, is used to subcool the high-pressure liquid leaving the condenser. Intracycle evaporative cooling was evaluated by a semi-theoretical simulation model and experimentally in an instrumented laboratory heat pump at the cooling mode operating condition typical for a water-to-water residential heat pump. The capacity, coefficient of performance (COP), pressures, and temperature profiles of refrigerant and heat-transfer fluid in the heat exchangers are reported. The laboratory measured improvement of the COP was 4.0% for R32/152a, 3.6% for R407C, and 1.8% for R23/152a.

Key words: air conditioning, building technology, Coefficient of Performance, heat pump, refrigeration, zeotropic mixtures

**Acknowledgments**

This study was sponsored by the U.S. Department of Energy, Office Building Technology. Mr. William Noel served as the project manager. The authors would like to thank Mr. Peter Rothfleisch and Mr. John Wamsley of NIST for their assistance. Financial support by LG Electronics, Inc. for Mr. Kim during his stay at NIST is also acknowledged.

**Table of Contents**


Abstract . . . . . iii

Acknowledgments . . . . . iv

Table of Contents . . . . . v

List of Figures . . . . . vi

Nomenclature . . . . . vi

1. Introduction . . . . . 1

2. Method 1: Subcooling Liquid Refrigerant With Two-Phase High-Quality Refrigerant Leaving Evaporator . . . . . 2
   2.1 Simulations . . . . . 3
   2.2 Laboratory Experiment . . . . . 4
      2.2.1 Test Facility . . . . . 4
      2.2.2 Test Procedure . . . . . 4
      2.2.3 Test Results . . . . . 5

3. Method 2: Subcooling Liquid Refrigerant With Refrigerant Bypassing Evaporator . . . . . 7
   3.1 Simulation Model . . . . . 7
   3.2 Simulation Results . . . . . 8

4. Concluding Remarks . . . . . 9

5. References . . . . . 10

6. APPENDIX . . . . . 19

**List of Figures**


Figure 1. Schematic of a system implementing intracycle evaporative cooling by Method 1 . . 11
Figure 2. Schematic of a system implementing intracycle evaporative cooling by Method 2 . . 11
Figure 3. Temperature profile during phase change at pressures corresponding to 7 °C bubble-point temperature . . . . . 12
Figure 4. Basic vapor compression cycle (1-2-3-4-5) and Method 1 cycle with intracycle evaporation cooling (1-2-3'-4'-5') . . . . . 12
Figure 5. Simulated COP of the Method 1 cycle referenced to the COP of the basic vapor compression cycle . . . . . 13
Figure 6. Simulated compressor power for the Method 1 cycle referenced to the compressor power of the basic vapor compression cycle . . . . . 13
Figure 7. Schematic of the Small Breadboard Heat Pump . . . . . 14
Figure 8. Measured COP of R22, R407C, R32/152a (50/50), R23/152a (20/80) . . . . . 15
Figure 9. Measured capacity of R22, R407C, R32/152a (50/50), R23/152a (20/80) . . . . . 16
Figure 10. Compressor suction pressure for R23/152a (20/80) . . . . . 17
Figure 11. Temperature profile of evaporator with R407C in the system without ic-hx . . . . . 17
Figure 12. Temperature profile of evaporator with R407C in the system with ic-hx . . . . . 17
Figure 13. Temperature profile of evaporator with R23/152 (20/80) in the system with ic-hx . . 17
Figure 14. Thermodynamic cycle for Method 2 of intracycle evaporative cooling ($P_{cond}$ = condenser pressure, $P_{evap}$ = evaporator pressure) . . . . . 18
Figure 15. Simulated COP for Method 2 cycle referenced to the COP of the basic vapor compression cycle . . . . . 18
Figure 16. Simulated capacity for Method 2 cycle referenced to capacity of the basic vapor compression cycle . . . . . 18
Figure 17. Simulated compressor power for Method 2 cycle referenced to compressor power of the basic vapor compression cycle . . . . . 18

**Nomenclature**

| | | |
|---|---|---|
| COP | = | Q/W ,coefficient of performance |
| EXP-AUX | = | auxiliary expansion device |
| $f_b$ | = | refrigerant mass flow rate flowing through the high-pressure side of the ic-hx divided by the total refrigerant mass flow rate (refrigerant mass flow rate through compressor) |
| HTF | = | heat-transfer fluid |
| h | = | enthalpy |
| IEC | = | intracycle evaporation cooling |
| ic-hx | = | intracycle heat exchanger |
| llsl-hx | = | liquid-line/suction-line heat exchanger |
| ODP | = | ozone depletion potential |
| P | = | pressure |
| Q | = | capacity |
| RPM | = | compressor speed (revolutions per minute) |
| UA | = | overall conductance |
| W | = | work |

Subscripts

| | | |
|---|---|---|
| cond | = | condenser |
| evap | = | evaporator |
| ref | = | reference |

## 1. Introduction

Throttling losses during adiabatic expansion have a dual negative effect on the Coefficient of Performance (COP) of the vapor-compression cycle. These losses reduce system capacity and result in increased cycle work due to the lost expansion work of the throttled refrigerant. Different modifications to the vapor compression cycle[1] (e.g., economizer, liquid-line/suction-line heat exchanger (lisl-hx), two-phase turbine, ejector) can be used to limit the expansion losses of single-component refrigerants and mixtures. Besides these methods, intracycle evaporative cooling (IEC) of the refrigerant leaving the condenser by the low-pressure evaporating refrigerant provides an additional opportunity for reducing throttling losses of zeotropic mixtures. This method can only be applied to zeotropes due to their temperature glide during phase change. The COP will be improved when heat transfer between the low-pressure and high-pressure refrigerant results in an increased evaporator pressure and smaller specific compression work. Intracycle evaporative cooling was originally discussed by Vakil[2].

Different quality ranges of the two-phase low-pressure refrigerant can be used for intracycle cooling. Mulroy et al.[3] studied the effect of intracycle cooling in a system with a three-passage evaporator using the entire quality range from the evaporator inlet to outlet. They directed the high-pressure refrigerant through one of these passages, counter-flow to the evaporating low-pressure refrigerant. The third passage was used by the heat-transfer fluid (HTF). Depending on mixture composition, the experimental data for R13/12 showed 5% to 10% COP improvement. In the same apparatus, little effect due to intracycle heat exchange was observed for R22/114.

Two other methods of applying the IEC are shown in Figures 1 and 2. In Method 1 (Figure 1), the high-pressure refrigerant is subcooled in the intracycle heat exchanger (ic-hx) by the two-phase refrigerant leaving the evaporator. This concept is related to the conventional liquid-line/suction-line heat exchange where superheated vapor is used to subcool the high-pressure liquid. In Method 2 (Figure 2), part of the high-pressure refrigerant is allowed to expand through the auxiliary expansion device (EXP-AUX). After the expansion (and a corresponding change of temperature), this refrigerant stream is used to subcool the main stream of the high-pressure refrigerant. As a result, refrigerant enthalpy and temperature at the inlet to the evaporator decrease increasing the specific refrigeration effect. These two methods for obtaining additional subcooling and reducing throttling irreversibilities are evaluated in this report.

The study considered four refrigerants: R22, R407C (R32/125/134a (23/25/52)), R32/152a (50/50), and R23/152a (20/80), with R22 being selected as a reference. These refrigerants were selected to support a water-to-water residential heat pump[4,5] project involving these fluids. Table 1 contains selected properties of the refrigerants studied. Except R22, the selected fluids have zero ozone

depletion potential (ODP). R407C and R32/152a have comparable linear glides. R23/152a has a larger and more nonlinear glide, as shown in Figure 3. Among the fluids tested, the R32/152a mixture has superior transport properties. All refrigerant properties in this study were calculated using subroutines from REFPROP[6]. These subroutines employed the Carnahan-Starling-DeSantis equation of state for calculating thermodynamic properties.

Table 1. Selected Properties of Tested Refrigerants at Atmospheric Pressure

| Refrigerant | Molar Mass (g/mol) | Bubble-Point/ Dew-Point (°C) | Temperature Glide (°C ) | Liquid Conductivity (W/m°C) | Liquid Viscosity (μP) |
|---|---|---|---|---|---|
| R22 | 86.47 | -40.8/-40.8 | 0.0 | 0.1286 | 3369 |
| R407C (23/25/52) | 86.20 | -43.8/-36.7 | 7.1 | 0.1380 | 4280 |
| R32/152a (50/50) | 58.34 | -43.7/-35.6 | 8.1 | 0.1804 | 3035 |
| R23/152a (20/80) | 66.81 | -51.7/-28.6 | 23.1 | 0.1590 | 3689 |

Note: The mixtures are defined by mass fractions.

## 2. Method 1: Subcooling Liquid Refrigerant With Two-Phase High-Quality Refrigerant Leaving Evaporator

Figure 1 shows a schematic of a system considered in this section to subcool the high-pressure refrigerant leaving the condenser. In this system, the high-pressure refrigerant leaving the condenser is subcooled by a low-pressure refrigerant leaving the evaporator at quality less than 1.0 (instead of superheated vapor, as it is done in the IIsl-hx system). Figure 4 presents a thermodynamic diagram for the basic refrigeration cycle and the modified, IEC cycle. For the modified cycle, the figure shows the limiting case of maximum heat transfer. This heat-transfer limit is indicated by the liquid (point 3') reaching the lowest temperature of the two-phase refrigerant in the evaporator (point 4'). It should be realized that the total benefit of intracycle heat exchange may have two sources: (1) an increased subcooling at the expansion device inlet and the system's response by increasing evaporator pressure and (2) a better use of the evaporator's heat-transfer area with two-phase refrigerant at the evaporator exit (no superheat). Figure 4 is simplified because it does not show an increased evaporator pressure as a result of intracycle heat transfer.

### 2.1 Simulations

The ic-hx cycle shown in Figure 1 was simulated using CYCLE-11, NIST's semitheoretical model.[7,4] CYCLE-11 performs simulations at imposed temperatures of the heat-transfer fluids (HTFs), which are specified at the inlet and outlet of the evaporator and condenser. In the version of CYCLE-11 used in this study, these heat exchangers are represented by their overall conductances (UA), which also are specified as input. It is assumed in the model that the heat-transfer conductance is constant throughout the heat exchangers regardless of refrigerant phase or quality. For the purpose of this study, the model was modified to enable simulating the cycle of interest.

The following list shows the input data for the simulations:

- temperature of HTF entering/leaving the evaporator, 13 °C/7 °C
- temperature of HTF entering/leaving the condenser, 29 °C/35 °C
- superheat at the compressor inlet, 0.0 °C
- polytropic compression efficiency, 0.85
- subcooling at the condenser outlet, 0.0 °C
- pressure drop in the condenser, 0.0
- pressure drop in the evaporator, 0.0
- pressure drop in the ic-hx, 0.0

Simulations were performed for several different vapor qualities leaving the evaporator and entering the ic-hx. Because saturated vapor was imposed at the compressor inlet for all simulations, different vapor qualities leaving the evaporator corresponded to different amounts of heat transferred between the low-pressure two-phase refrigerant and the high-pressure subcooled liquid. Additional simulations were conducted for a basic system (not involving the ic-hx) to obtain a performance reference point.

Figure 5 shows the coefficient of performance (COP) referenced to that of the basic cycle. Implementation of the ic-hx did not change the performance of R22, but it improved the performance of the mixtures. The maximum COP of mixtures occurs at the highest amount of heat transferred in the ic-hx, which corresponds to the lowest quality of refrigerant leaving the evaporator. For this condition, the COP improvement is similar for all three mixtures (approximately 3%). The compressor power changed insignificantly with the use of ic-hx, as shown in Figure 6. This implies that the COP improvement was caused by an increase in capacity.

It should be noted that R32/152a and R407C have a linear temperature glide similar in magnitude to that of the heat-transfer fluids. On the other hand, the glide of R23/152 is nearly twice this magnitude and highly nonlinear in the low quality region (Figure 3), which results in a glide mismatch. The similar COP improvement potential for these three mixtures indicates the

importance of glide matching between refrigerant and heat-transfer fluid, and it discounts the significance of a high glide as a stand alone merit.

### 2.2 Laboratory Experiment

#### 2.2.1 Test Facility

The study was performed using an experimental apparatus referred to as a Small Breadboard Heat Pump (SBHP). This apparatus has been used in a few previous NIST projects, starting with the investigation by Pannock and Didion.[8] A few modifications were made to the original apparatus to facilitate studying the ic-hx cycle. Figure 7 shows a schematic of the modified system. The refrigerant side of the SBHP consisted of the compressor, condenser, intracycle heat exchanger, expansion device, and evaporator. The system employed an open, two-cylinder reciprocating compressor of 45 $cm^3$ total displacement. The inverter maintained compressor speed constant at 800 RPM during all tests. Commercially available torque and RPM transducers were used to measure the revolution speed and torque. All four refrigerants were tested with the same mineral oil in the compressor.

The condenser and evaporator had a counterflow tube-in-tube configuration and used a water/ethylene-glycol (60/40) mixture as the heat transfer fluid. After leaving the condenser, the refrigerant flowed either directly to the expansion device, or first to the ic-hx and then to the expansion device. From the evaporator, the refrigerant flowed to the compressor either directly or through the low-pressure side of the ic-hx. The ic-hx assembly comprised four identical heat exchangers, which could be brought on line independently to vary the heat-transfer area.

Refrigerant temperature and pressure were measured by thermocouples and pressure transducers placed in key locations of the refrigerant loop. Additionally, thermocouples were installed throughout the heat exchangers to measure the temperature profiles of the refrigerant and HTF. The thermocouples were type T and were surface-mounted. System capacity was measured on the HTF side. A Coriolis-type mass flow meter provided HTF mass flow rate. Temperature change of the HTF across the heat exchangers was measured by ten-junction thermopiles located at the inlet and outlet of the condenser and evaporator. A data acquisition/control unit connected to a personal computer was used to control system operation and test conditions as well as for collection of test data. A summary of the uncertainty analysis is given in the Appendix.

#### 2.2.2 Test Procedure

The tests were conducted at the same HTF temperatures as those used in the CYCLE-11 simulations. The inlet temperatures were controlled by electric heaters, and the outlet temperatures were controlled by adjusting HTF mass flow rates. Refrigerant subcooling at the condenser outlet was maintained at 4 °C ± 2 °C for all tests. On the low-pressure side, the refrigerant superheat at

the compressor inlet was maintained at 5 °C ± 2 °C. For the system with the ic-hx, the refrigerant leaving the evaporator was two-phase. This was confirmed by a combination of visual observation through the sight glass and measurement of the refrigerant pressure and temperature profile in the evaporator. The quality of refrigerant leaving the evaporator was calculated from the enthalpy change of the subcooled liquid in the ic-hx assuming not heat transfer to the ambient air. The refrigerant charge and expansion valve opening were adjusted to obtain the specified superheat and subcooling for a given combination of intracycle heat exchangers. System operating parameters were recorded after the HTF temperatures were maintained within ±0.1 °C of the temperature set points for at least 15 minutes.

The experimental rig was charged by weight from containers holding individual refrigerants. A gas chromatograph was used for determining composition of the mixtures. The analysis was performed using a small amount of vapor taken from the compressor discharge line after the system reached steady-state operation. The circulating mass compositions were 24/27/59 for R32/125/134a, 47/53 for R32/152a, and 23/77 for R23/152a. The deviations of these compositions from those employed in simulations were not large enough to make appreciable impact on performance (this was verified with additional CYCLE-11 simulations). Therefore, for simplicity of presentation, the rounded compositions from simulation runs are uniformly used to identify the fluids studied.

### 2.2.3 Test Results

The test results for COP and capacity are presented graphically in Figures 8 and 9. In these figures, the horizontal dotted line denotes the reference performance of a system without the ic-hx for the same refrigerant. The combined uncertainty (95% confidence level) for COP and capacity was estimated to be 4.2% and 4.3%, respectively. Among the four fluids tested, the R32/152a mixture had the highest reference COP (5.15), followed by that of R22 (4.94), R407C (4.67), and R23/152a (4.41). The R23/152a mixture displayed a low COP despite having a much lower capacity than the other fluids. The highest reference capacity was measured for R407C. The reference capacities of R22 and R32/152a were within 3.3% of that of R407C, and the reference capacity for R23/152a was 23% lower. All three mixtures benefited from the ic-hx, while the COP of R22 deteriorated, as shown in Figure 8. The COP increases for mixtures were 4.0% for R32/152a, 3.6% for R407C, and 1.8% for R23/152a. These COP increases were calculated using the average of the COP for the tests with 88-90% refrigerant quality at the evaporator exit. The data points for 100% evaporator outlet quality represent the results from a few tests with different superheats at the evaporator exit. Because of the superheat, the system capacities were lower, which resulted in the low COPs. Also, more superheated (higher temperature) vapor required more specific compression work because of a lower density. This was an additional negative effect on the system COP, although not as significant as that due to the decrease in evaporator capacity.

Figure 9 shows the measured capacities. The capacity of R22 was unaffected by the use of the ic-hx, but the mixture capacities were increased. Compared with the reference value for the tests without the ic-hx, the maximum capacity improvement is approximately 7.0% for R32/152a (50/50), 3.4% for R407C, and 4.4% for R23/152a (20/80).

The use of the ic-hx did not significantly affect the pressure in the condenser. However, the suction pressure increased with the amount of heat transferred in the ic-hx. Figure 10 shows the compressor suction pressure for R23/152a. The pressure trend shown in this figure is typical for other mixtures. An increase of the suction pressure reduces the specific work needed to compress the refrigerant to the condenser pressure, improving system efficiency. As expected, no change of suction (evaporator) pressure was measured for R22.

Figures 11, 12, and 13 present HTF and refrigerant temperature profiles in the evaporator. The profiles in the evaporator are of substantial interest because they are affected by the ic-hx. Refrigerant temperatures were measured by thermocouples surface-mounted on the return bends of the heat exchangers. HTF temperatures were measured by thermocouples placed in stainless steel wells at the return bends. Due to the compact design of the heat exchangers, the HTF temperature measurements were affected by conduction with refrigerant passages. This heat transfer manifests itself in a seesaw temperature profile, which is particularly visible for the HTF. Even with this shortcoming, the temperature profiles can be used for a qualitative comparison. Figures 11 and 12 show the temperature profiles for the basic system and ic-hx system working with R407C. The refrigerant profile for the ic-hx system does not have a superheated vapor spike because vapor superheating takes place in the ic-hx. The temperature of the evaporating refrigerant is higher in the ic-hx system than in the basic system.

R23/152a achieved the lowest COP among the tested fluids in spite of the lowest capacity. Typically, a low-capacity refrigerant has a better COP than the higher-capacity fluid when evaluated in a given system[9]. The poor performance of R23/152a, both in the basic and modified cycle, can be explained by the mismatched temperature profiles in the evaporator and condenser. Figure 13 shows that R23/152a displays significant nonlinearity in the low-quality region in the evaporator. A similar nonlinear temperature profile was also present in the condenser where a strong pinch point occurred.

The preceding observation regarding the performance of R32/152a can be generalized to other high-glide zeotropic mixtures. It appears that high-glide binary mixtures, like R23/152a having more than 20 °C glide, will inherently have a very nonlinear temperature profile (Figure 3). Such mixtures will perform poorly in heat exchangers because common heat-transfer fluids have a nearly constant heat capacity and linear temperature profile. The mismatch in temperature profiles will result in

significant heat-transfer irreversibilities, which will cause the poor system performance. A properly formulated ternary or higher-order mixture may exhibit a less nonlinear temperature profile while having a high glide during phase change[9].

## 3. Method 2: Subcooling Liquid Refrigerant With Refrigerant Bypassing Evaporator

### 3.1 Simulation Model

Method 2 of evaporative cooling is realized in a system presented in Figure 2. In this system, part of the high-pressure refrigerant is allowed to bypass the evaporator and expand through the auxiliary expansion device (EXP-AUX). After expansion, this refrigerant stream subcools the main stream of high-pressure refrigerant and then flows to the suction line. As a result, the refrigerant flowing to the evaporator has a lower mass flow rate, but larger specific refrigerating effect. The evaporator and condenser pressures also change, which affects the system capacity and COP.

The system shown in Figure 2 was simulated using NIST's semitheoretical model, CYCLE-11. The model was modified to facilitate simulating the intracycle heat exchange. The following list shows the input data for the simulations:

- temperature of HTF entering/leaving the evaporator, 13 °C / 7 °C
- temperature of HTF entering/leaving the condenser, 29 °C / 35 °C
- polytropic compression efficiency, 0.85
- subcooling at the condenser outlet, 0.0 °C
- superheat at the evaporator outlet, 10 °C
- pressure drop in the condenser, 0.0
- pressure drop in the evaporator, 0.0
- pressure drop in the ic-hx, 0.0

The model allowed for variation of the fraction of refrigerant bypassing the evaporator and flowing through the low-pressure side of the ic-hx. This fraction of refrigerant flow is denoted by $f_b$. For small values of $f_b$, the bypass refrigerant reaches the temperature of saturated liquid leaving the condenser. This state is shown in Figure 14 as point 5hx. For increasing values of $f_b$, the enthalpy of the refrigerant entering the evaporator moves toward the liquid saturation line. As a limit, this enthalpy will approach the enthalpy of point 5. At this point, the liquid entering the main expansion device is subcooled to the temperature of the expanded bypass refrigerant at point 4hx. For further increases of $f_b$, the refrigerant passing through the evaporator will have a lower heat-capacity flow rate than the refrigerant stream bypassing the evaporator, and it will limit the amount of heat that can be transferred in the ic-hx. Consequently, at larger values of $f_b$, the bypass refrigerant will not reach the temperature of saturated liquid leaving the condenser (temperature of point 3), but will progressively approach the temperature of the saturated vapor at the evaporator pressure. Even

further increases of $f_b$ will cause the bypass refrigerant to leave the ic-hx in two-phase.

In the simulations, the refrigerant state at the evaporator outlet (point 6) was constrained by the specified evaporator superheat of 10 °C, and the refrigerant enthalpy at the exit of the bypass was constrained by the amount of heat transfer in the ic-hx. The refrigerant state at the compressor inlet (point 1) was determined by the evaporator pressure and the enthalpy calculated for the mixing streams: $h_1 = (1-f_b)\cdot h_6 + f_b \cdot h_{5hx}$, where $h_6$ is refrigerant enthalpy leaving the evaporator (see Figure 2 for designation numbers). Simulations were performed for $f_b$ values for which the refrigerant entering the compressor was either superheated vapor or high quality two phase.

### 3.2 Simulation Results

Results from simulation runs are presented in Figures 15, 16, and 17. The abscissa in these figures is the refrigerant mass flow rate flowing through the evaporator as a fraction of the total refrigerant mass flow rate flowing through the compressor, $(1-f_b)$. The presented data are for superheated and saturated vapor entering the compressor. The value of $f_b$ for which saturated vapor enters the compressor varies slightly among refrigerants. For R22, R32/152a, and R23/152a, this occurs at $(1-f_b)$ approximately equal to 0.75, while for R407C zero superheat is reached for $(1-f_b)$ smaller than 0.7.

Figure 15 shows the COP referenced to the coefficient of performance of the basic cycle (without the ic-hx), $COP_{ref}$. The COP trend is similar for all fluids. The COP increases with decreasing $(1-f_b)$ until the superheat of the bypass refrigerant becomes zero (bypass superheat is not shown in the figure). A drastic drop of COP occurs for two-phase refrigerant leaving the ic-hx. The performance of R407C and R32/152a mixtures improved the most because of the intracycle heat exchange. The improved COP of R407C extends to lower values of $(1-f_b)$. It is reasonable to speculate that the higher heat capacity of R407C allows for this extension. The COP benefit for R23/152a and R22 is negligible. The R23/152a mixture has a highly nonlinear temperature profile in two-phase in the low-quality range (Figure 3), and it can be blamed for the small improvement of COP. Since R22 does not change temperature during phase change, its COP improvement was caused only by a typical liquid-line/suction-line heat exchange effect. Figures 16 and 17 complement Figure 15 with capacity and compressor power data.

The observed magnitude of COP improvement and its sensitivity to the refrigerant stream split between the evaporator and ic-hx present practical limits for application of this modified refrigeration cycle. In a real machine, the fraction of refrigerant bypassing the evaporator would have to be tightly controlled to avoid a performance penalty. Because of the narrow range of $f_b$ for which the COP improvement occurs and the possibility of incurring a COP penalty when $f_b$ is outside this range, this method was not studied further in the laboratory.

## 4. Concluding Remarks

This study evaluated two methods of intracycle evaporative cooling of high-pressure refrigerant to improve the performance of the vapor compression cycle. In Method 1, the refrigerant is not fully evaporated in the evaporator, and the remaining refrigeration effect is used for evaporative cooling. In Method 2, the refrigerant stream leaving the condenser is split. A small fraction of the total refrigerant flow is expanded in an auxiliary restrictor, and the refrigeration effect is used to subcool the refrigerant flowing to the main expansion device and evaporator. Both streams merge before entering the compressor. The benefit of evaporative cooling was evaluated for the cooling mode condition of a water-to-water heat pump. In general, intracycle evaporative cooling of the refrigerant leaving the condenser improves the performance of zeotropic mixtures, but the potential of performance improvement and the complexity of implementation of evaporative cooling are different for the two methods studied.

For Method 1, laboratory tests showed that the COP of the zeotropic mixtures improved with evaporative cooling while the performance of R22 did not. The COP increase was 4.0% for R32/152a (50/50), 3.6% for R407C, and 1.8% for R23/152a (20/80). The cooling capacity increased by 7.0% for R32/152a, 3.4% for R407C, and 4.4% for R23/152a. Although the combined uncertainty at 95 percent level was calculated to be 4.2% for capacity and 4.3 for COP, the agreement between the measured performance trends and those obtained from simulations provides confidence in the test data. It can be inferred that intracycle evaporative cooling was not the only reason for the improved performance of the ic-hx system; most likely the elimination of superheated refrigerant at the evaporator exit and a corresponding change in the refrigerant-side heat-transfer coefficient also contributed to the performance change. On an absolute scale, R32/152a (50/50) showed the best COP, followed by R22, R407C, and R23/152a (20/80).

Method 2 of evaporative cooling was evaluated by simulations. The COP improved 3% for R407C and R32/152a, and less than 1% improvement was obtained for R23/152a and R22. The maximum value of COP occurred at approximately 80/20 split between the refrigerant flowing through the evaporator and that used for evaporative cooling. At a lower fraction of the refrigerant used in the evaporator, the system's performance decreased sharply. Because of this performance characteristic and expected difficulty with field implementation, evaporative cooling by Method 2 was not investigated in the laboratory.

The results obtained for Method 1 and Method 2 show the importance of glide matching between the refrigerant and heat-transfer fluid. The worst performer, R23/152a, had the temperature glide more than twice as high as the HTF and had a significant nonlinearity in the phase-change temperature profile in the low-quality region. The best performers, R32/152a and R407C, achieved the best COP in the basic cycle and the best COP improvement in the cycles modified to implement

evaporative cooling. Both mixtures had an almost linear temperature glide which corresponded in magnitude to the glide of the HTF in the evaporator and condenser.

## 5. References


1. Domanski, P.A., "Minimizing Throttling Losses in the Refrigerant Cycle," Proceedings of the Int. Congr. Refrig., The Hague, The Netherlands, Vol. 4b, 1995.
2. Vakil, H.B., "Thermodynamics of heat exchange in refrigeration cycles with non-azeotropic mixtures. Part II, Suction heat exchange and evaporative cooling of capillary," Proceeding XVI Int. Congr. Refrig., Paris, France, IIR, Commission B1, 1983.
3. Mulroy, W., Kauffeld, M., McLinden, M., and Didion, D., "An Evaluation of Two Refrigerant Mixtures in a Breadboard Air Conditioner," Proceedings of the IIR-Purdue Conference, IIR, Paris, France, 1988.
4. Domanski, P.A., Didion, D.A., Mulroy, W.J., and Parise, J., "A Simulation Model and Study of Hydrocarbons Refrigerants for Residential Heat Pump Systems," Proceedings o the International Conference on New Applications of Natural Fluids in Refrigeration and Air Conditioning, Hanover, Germany. IIR, Paris, France, 1994.
5. Choi, D.K., Domanski, P.A., and Didion, D.A., "Laboratory Evaluation of Flammable Refrigerants for Application in a Water-to-Water Heat Pump," NISTIR (to be published), National Institute of Standards and Technology, Gaithersburg, MD, 1995.
6. Gallagher, J., McLinden, M.O., Morrison, G., and Huber, M., "NIST Standard Reference Data Base 23, Version 4.01" (REFPROP), National Institute of Standards and Technology, Gaithersburg, MD, USA, 1993.
7. Domanski,P.A. and McLinden,M.O., "A Simplified Cycle Simulation Model for the Performance Rating of Refrigerants and Refrigerant Mixtures,"Int. J. Refrig., Vol 15, No.2, 1992.
8. Pannock, P.A. and Didion, D.A., "The Performance of Chlorine-Free Binary Zeotropic Refrigerant Mixtures in a Heat Pump," NISTIR 4748, National Institute of Standards and Technology, Gaithersburg, MD, 1992.
9. Mulroy, W.J., Domanski, P.A., and Didion, D.A., "Glide matching with binary and ternary zeotropic refrigerant mixtures," Part 1, An experimental study, Int. J. Refrig., Vol 17, No. 4, 1994.

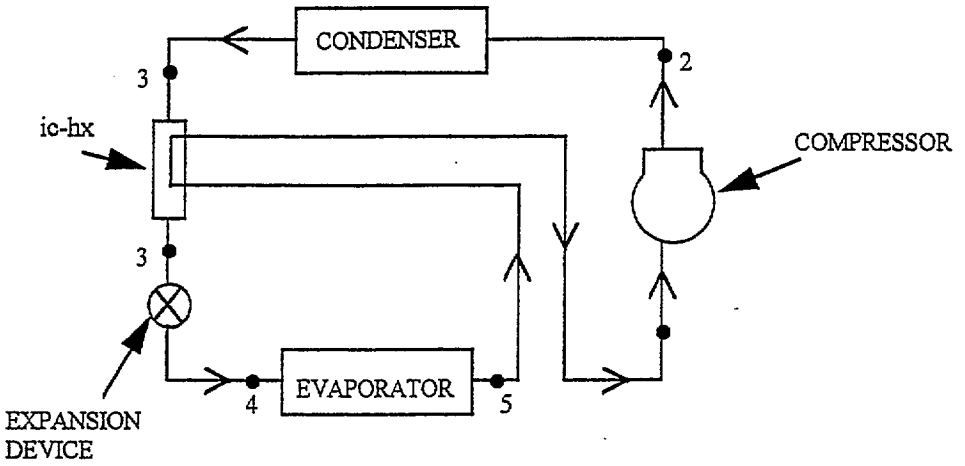


Figure 1. Schematic of a system implementing intracycle evaporative cooling by Method 1

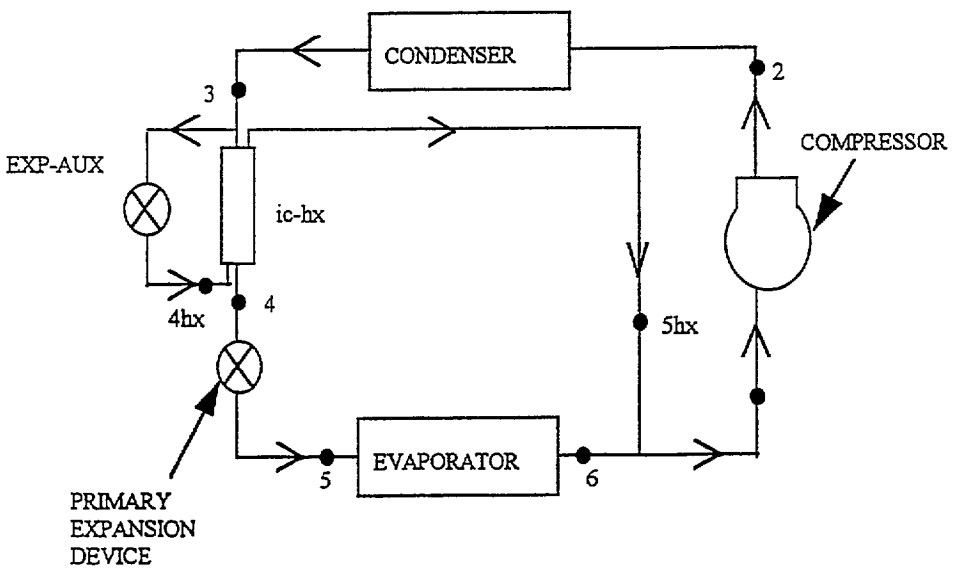


Figure 2. Schematic of a system implementing intracycle evaporative cooling by Method 2

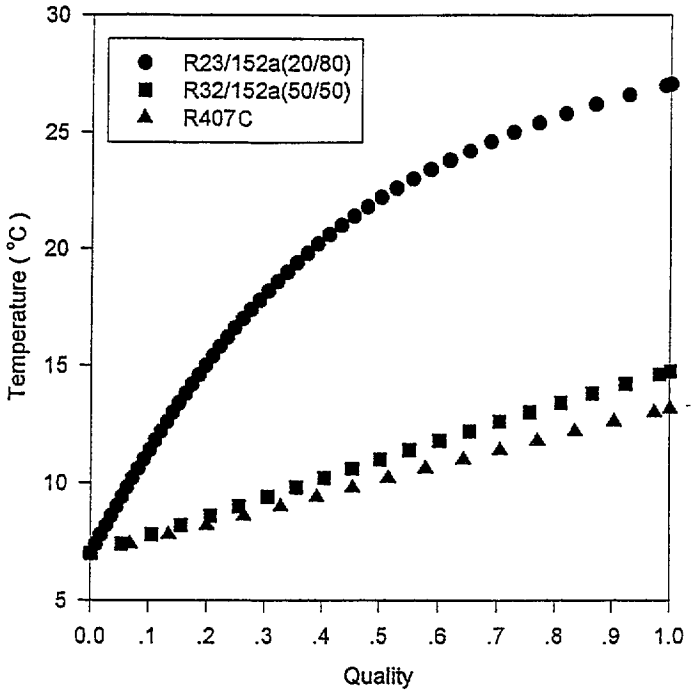


Figure 3. Temperature profile during phase change at pressures corresponding to 7°C bubble-point temperature

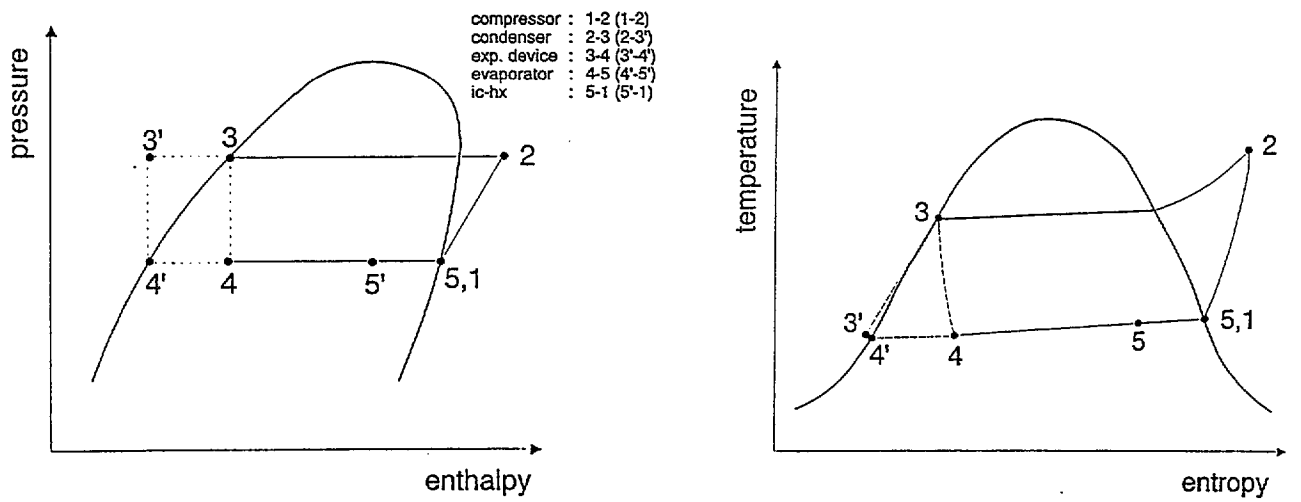


Figure 4. Basic vapor compression cycle (1-2-3-4-5) and Method 1 cycle with intracycle evaporation cooling (1-2-3'-4'-5')

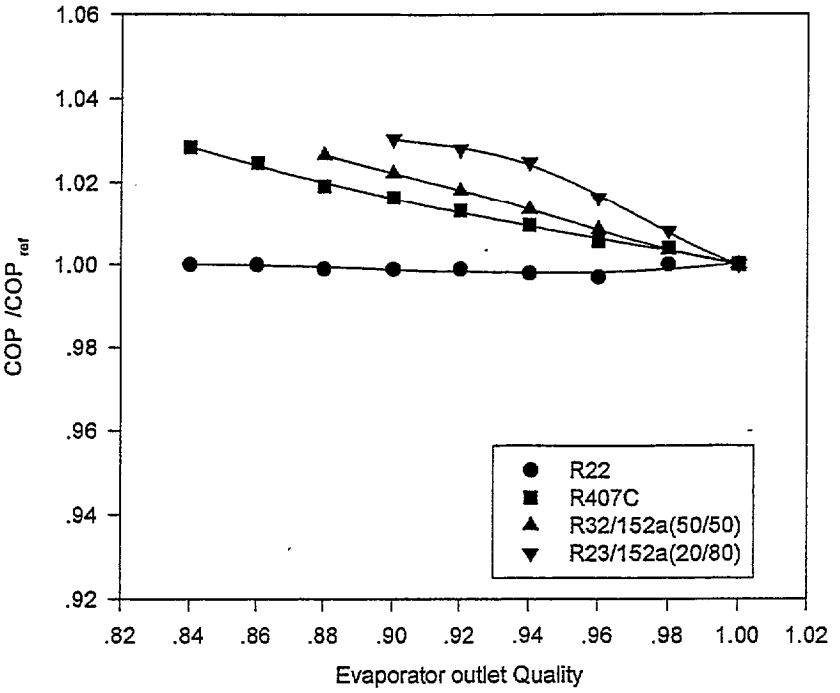


Figure 5. Simulated COP of the Method 1 cycle referenced to the COP of the basic vapor compression cycle

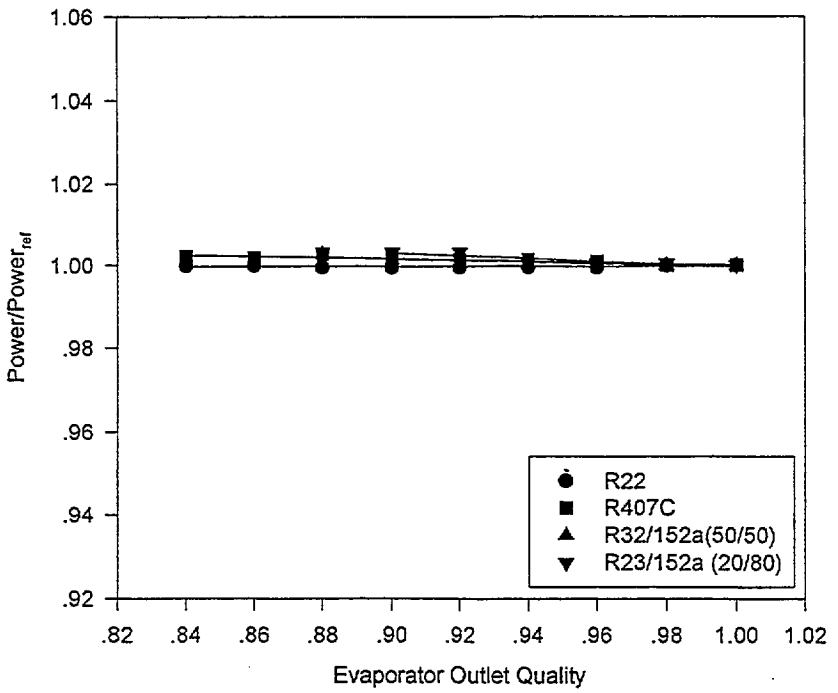


Figure 6. Simulated compressor power for the Method 1 cycle referenced to the compressor power of the basic vapor compression cycle

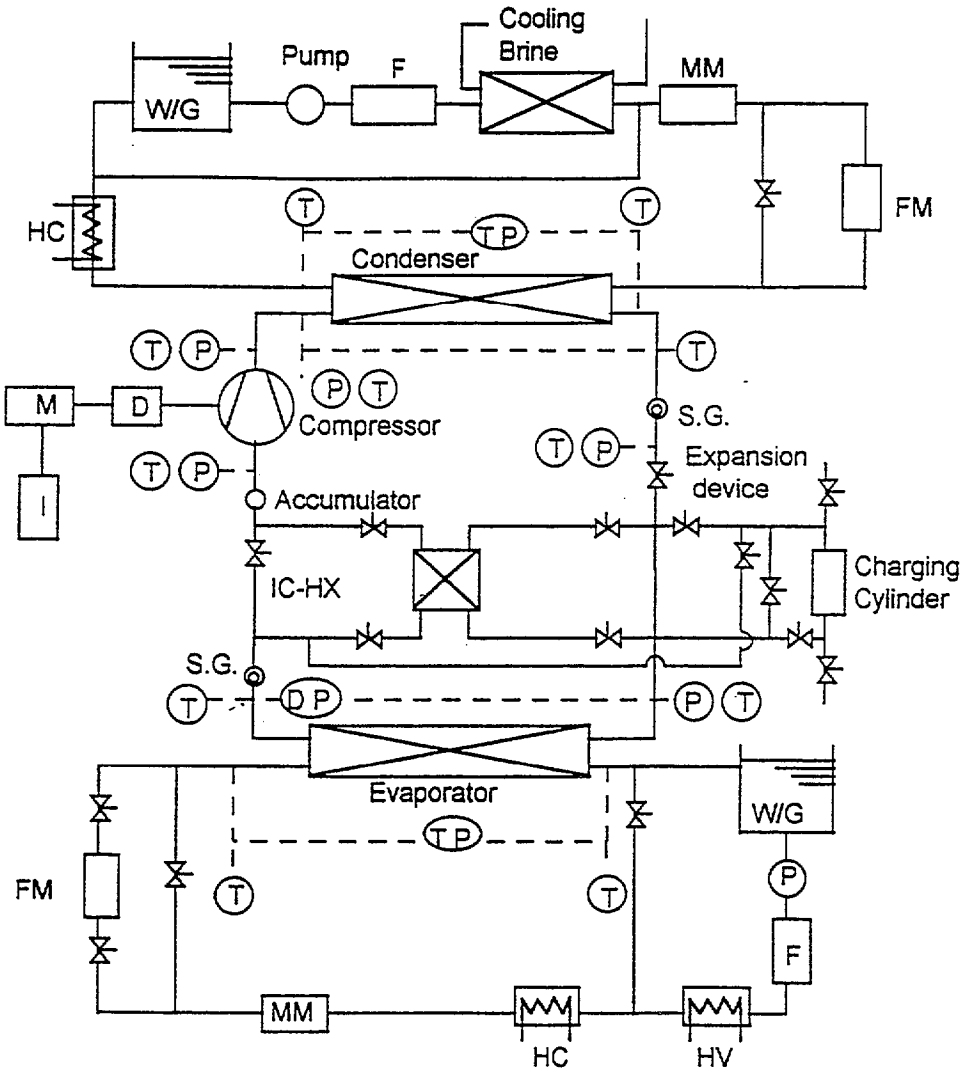


P Pressure
T Temperature
TP Thermopile
DP Pressure Difference
W / G Water / Glycol
IC- HX Intracycle heat exchanger

M Motor
I Inverter
D Dynamometer
F Filter

FM Volume Flowmeter
MM Mass Flowmeter
HC Heat Constant
HV Heat Variable
S.G. Sight Glass

Figure 7. Schematic of the Small Breadboard Heat Pump

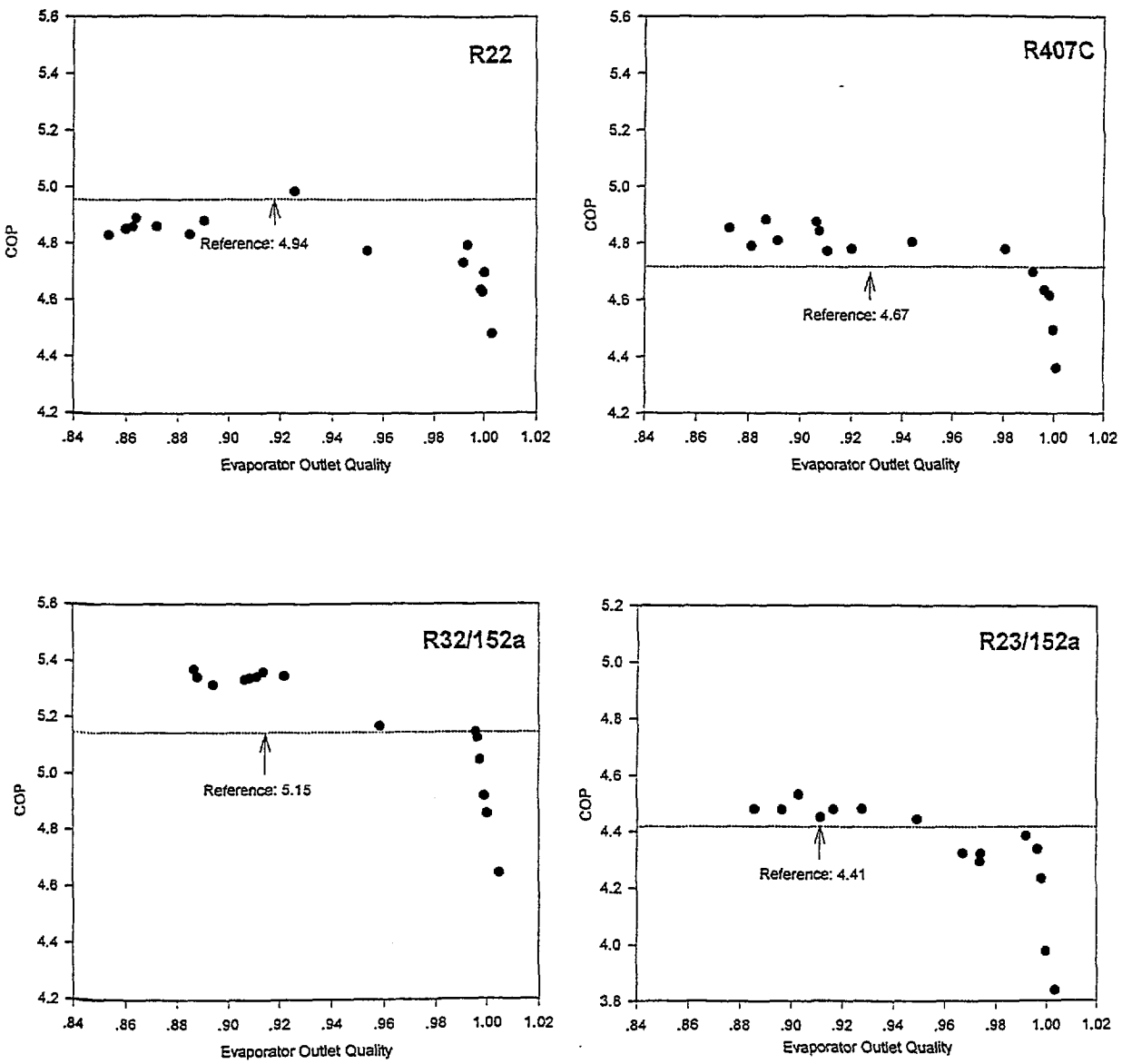


Figure 8. Measured COP of R22, R407C, R32/152a (50/50), R23/152a (20/80)

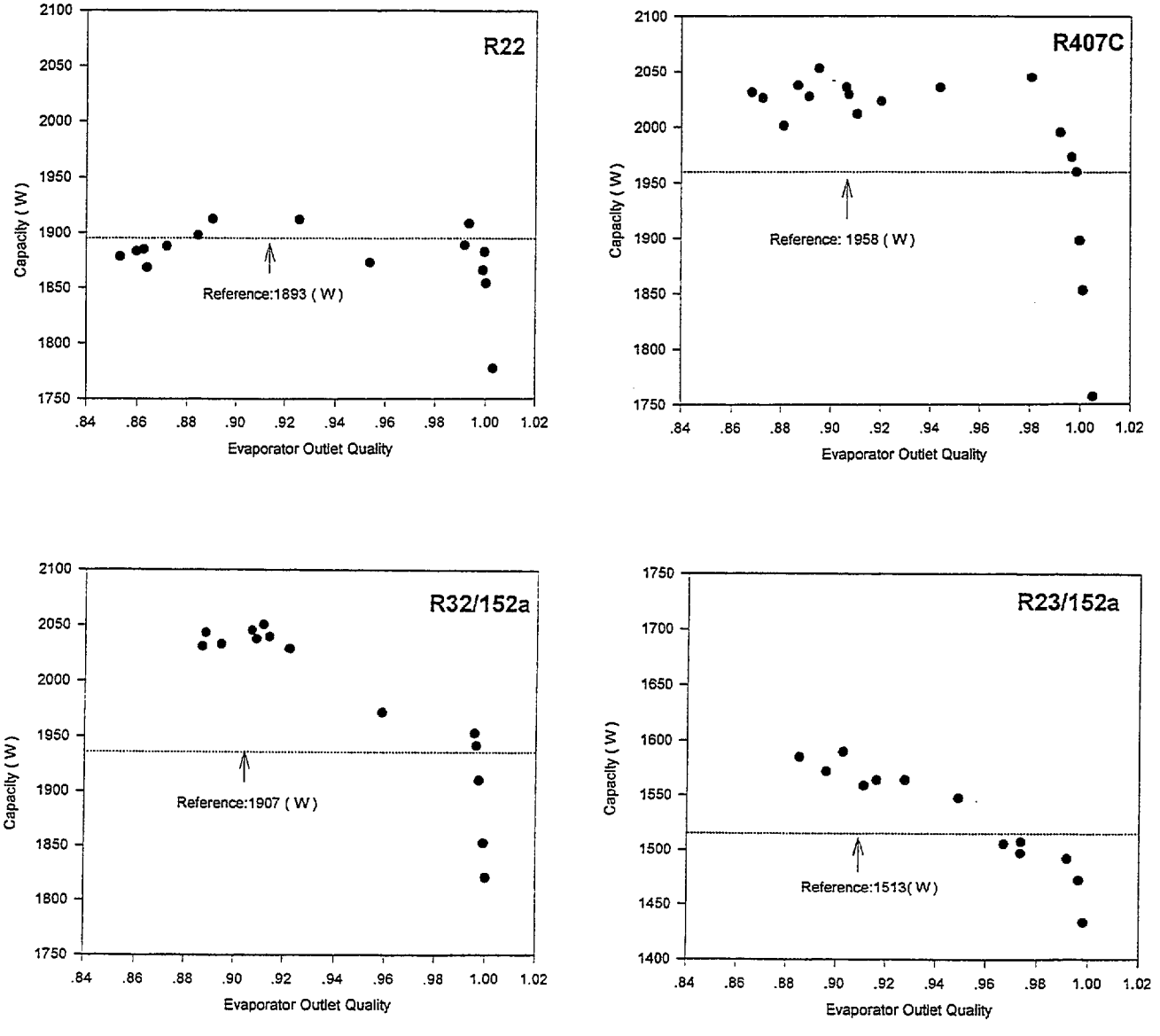


Figure 9. Measured capacity of R22, R407C, R32/152a (50/50), R23/152a (20/80)

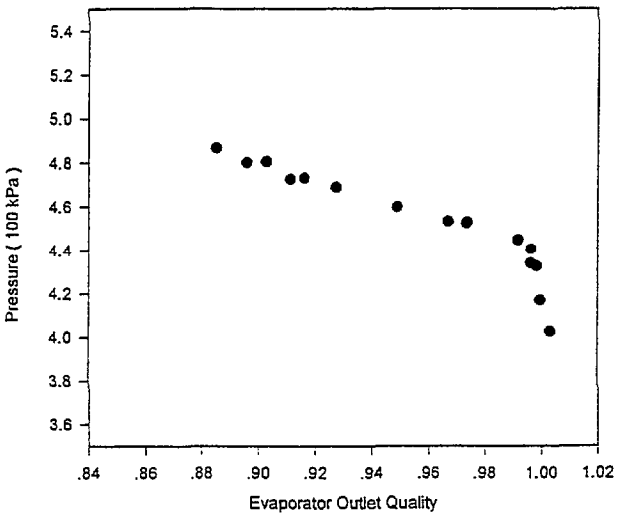


Figure 10. Compressor suction pressure for R32/152a (20/80)

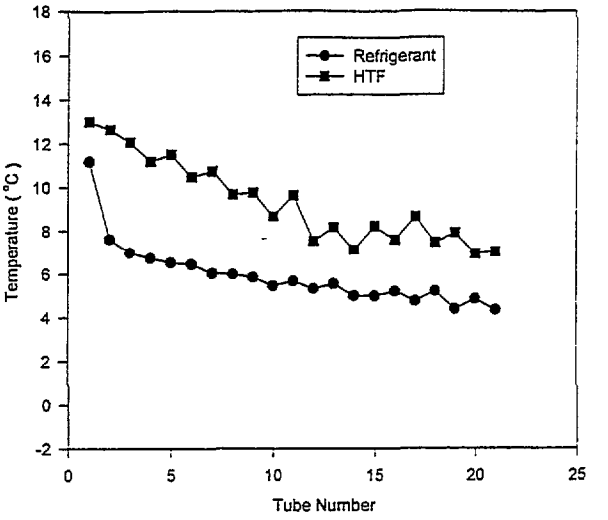


Figure 11. Temperature profiles of evaporator with R407C in the system without ic-hx

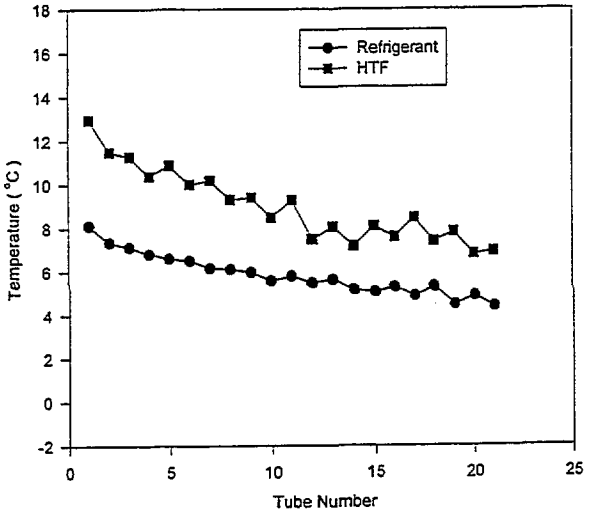


Figure 12. Temperature profiles of evaporator with R407C in the system with ic-hx

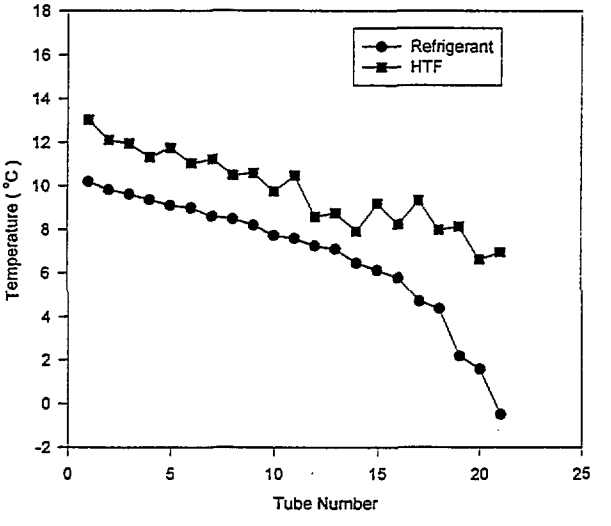


Figure 13. Temperature profiles of evaporator with R23/152a (20/80) in the system with ic-hx

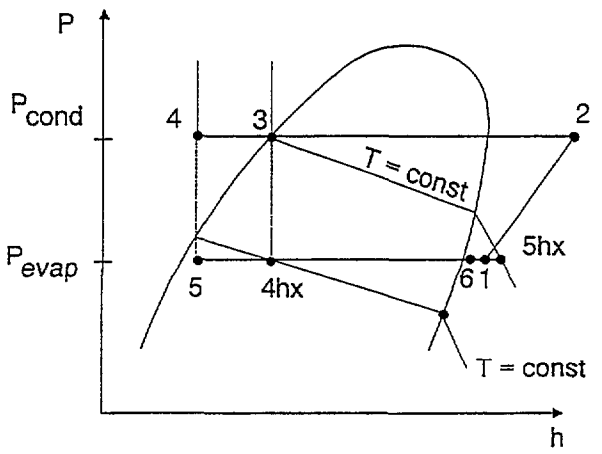


Figure 14. Thermodynamic cycle for Method 2 of intracycle evaporative cooling ($P_{cond}$ = condenser pressure $P_{evap}$ = evaporator pressure)

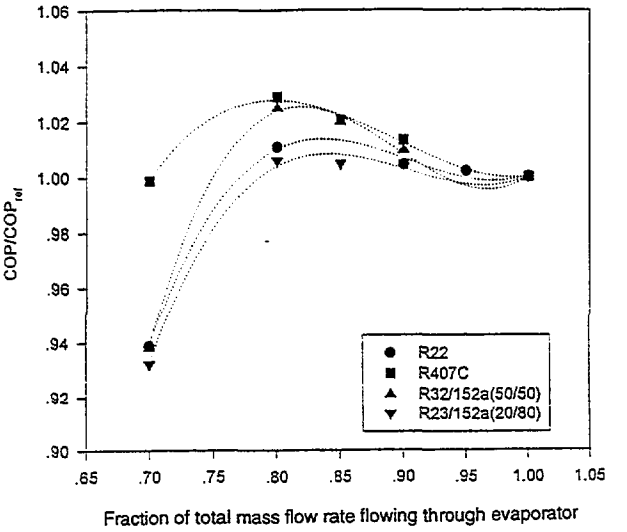


Figure 15. Simulated COP for Method 2 cycle referenced to the COP of the basic vapor compression cycle

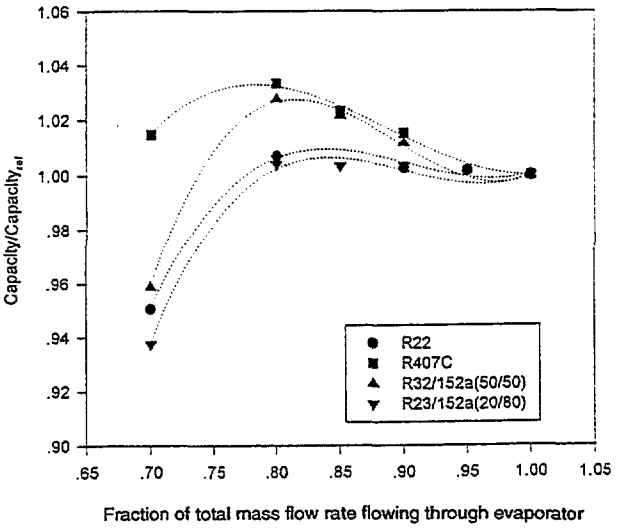


Figure 16. Simulated capacity for Method 2 cycle referenced to capacity of the basic vapor compression cycle

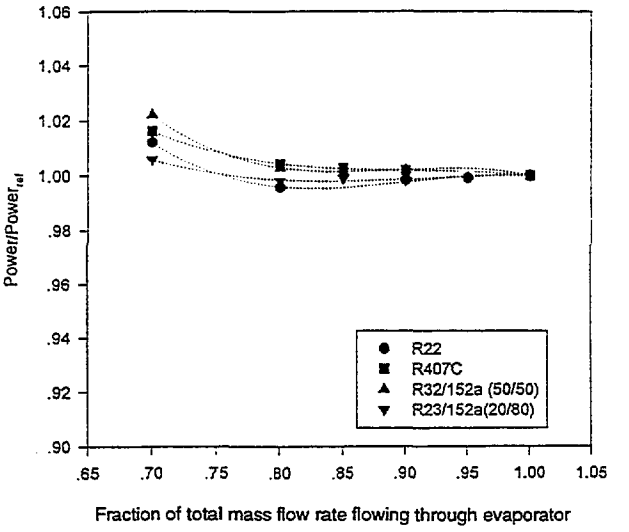


Figure 17. Simulated compressor power for Method 2 cycle referenced to compressor power of the basic vapor compression cycle

## APPENDIX

### Data Uncertainty Information

A detailed uncertainty analysis for the Small Breadboard Heat Pump was presented by Pannock and Didion[8]. Since the current investigation used the same apparatus and instrumentation, their methodology was used to provide the data uncertainty information. The only deviation from the referenced method was the use of an estimate for the uncertainty of the measurement of the HTF temperature difference. Based on the calibration measurements of a similar setup consisting of a thermopile and the same data acquisition system, a conservative estimate of 0.1 °C has been selected. Table A1 contains the summary of uncertainty analysis calculated for the reference test with R22.

Table A1. Summary of uncertainty analysis

| | Parameter value and uncertainty* | |
|---|---|---|
| HTF temperature difference between evaporator inlet and outlet | 6.0 °C ± 0.1 °C | (±1.7%) |
| Mass flow rate | 0.108 kg/s ± $4.3 \cdot 10^{-4}$ kg/s | (±0.4%) |
| HTF specific heat | 3.495 kJ/(kg·°C) ± 0.1 kJ/(kg·°C) | (±0.3%) |
| Compressor power | 383.2 W ± 4.5 W | (±1.2%) |
| Capacity | 1893 W ± 80 W | (±4.2%) |
| Coefficient of Performance | 4.94 ± 0.21 | (±4.3%) |

* Approx. 95 percent confidence level